communications physics

ARTICLE

https://doi.org/10.1038/s42005-021-00554-y OPEN

Controlled creation and decay of singly-quantized vortices in a polar magnetic phase

Y. Xiao[1,5], M. O. Borgh[2], L. S. Weiss[1,6], A. A. Blinova[1,3], J. Ruostekoski[4] & D. S. Hall[1✉]

Quantized vortices appear in physical systems from superfluids and superconductors to liquid crystals and high energy physics. Unlike their scalar cousins, superfluids with complex internal structure can exhibit rich dynamics of decay and even fractional vorticity. Here, we experimentally and theoretically explore the creation and time evolution of vortex lines in the polar magnetic phase of a trapped spin-1 ^{87}Rb Bose–Einstein condensate. A process of phase-imprinting a nonsingular vortex, its decay into a pair of singular spinor vortices, and a rapid exchange of magnetic phases creates a pair of three-dimensional, singular singly-quantized vortex lines with core regions that are filled with atoms in the ferromagnetic phase. Atomic interactions guide the subsequent vortex dynamics, leading to core structures that suggest the decay of the singly-quantized vortices into half-quantum vortices.

[1] Department of Physics and Astronomy, Amherst College, Amherst, MA, USA. [2] Faculty of Science, University of East Anglia, Norwich, UK. [3] Department of Physics, University of Massachusetts Amherst, Amherst, MA, USA. [4] Department of Physics, Lancaster University, Lancaster, UK. [5] Present address: Department of Electrical and Computer Engineering, University of Michigan, Ann Arbor, MI, USA. [6] Present address: Department of Physics and James Franck Institute, University of Chicago, Chicago, IL, USA. ✉email: dshall@amherst.edu

Vortices in superfluids with internal degrees of freedom, such as those existing within spinor Bose–Einstein condensates (BECs)[1,2] and superfluid liquid He-3[3,4], exhibit a much richer phenomenology than do simple line vortices in scalar superfluids. Notable examples abound, including vortices with fractional charges[5–11], vortices with like charges that sum to zero[12], vortices with charges that do not commute[13–19], and nonsingular textures with angular momentum[20–25]. These features, among others, hint at their highly counter-intuitive dynamics.

The symmetry properties of the superfluid order parameter determine its magnetic phases and topologically permissible vortex excitations[1]. The ground state of a spin-1 system, for example, exhibits two phases: a polar phase, which minimizes the total spin and is characterized by a nematic axis $\hat{\mathbf{d}}$ and condensate phase τ; and a ferromagnetic phase, which maximizes the total spin and is characterized by a vector triad. In turn, the ground-state phase of an atomic BEC in zero magnetic field is determined by the nature of the interatomic interactions, which are themselves polar (e.g., in ^{23}Na) or ferromagnetic (e.g., in ^{87}Rb)[1]. Interactions at the atomic scale thus influence both the type and destiny of vortices within the condensate.

In the polar phase, a singly-quantized vortex (SQV) with 2π phase winding is unstable against splitting into a pair of half-quantum vortices (HQVs), each with π phase winding. This unusual possibility was proposed and analyzed in ref. [8] and subsequently observed experimentally within a ^{23}Na BEC in an effectively two-dimensional trapping geometry[9,26]. The core of a vortex in superfluid ^{3}He-B has similarly been predicted[27,28] and observed[29] to consist of two HQVs; and, more recently, HQVs have been observed in the ^{3}He polar phase[10].

Here, we describe the controlled creation and subsequent time evolution of a pair of three-dimensional (3D) singular SQVs in the polar phase of a spin-1 ^{87}Rb BEC with ferromagnetic interatomic interactions. In contrast to techniques that randomly nucleate vortices throughout the superfluid by, e.g., stirring[9,30,31] or rapid cooling through the superfluid transition[32–34], our experiment makes use of a deliberately applied strong bending of a nonsingular spin texture to generate a pair of singular, singly-quantized ferromagnetic-phase [SO(3)] vortices with polar-phase filled cores at a specific location within the BEC[12]. We then swiftly exchange the polar and ferromagnetic phases using a trio of microwave transitions that appropriately reapportion the spinor components of the system. The resulting pair of polar SQVs possesses a topological interface[35,36] between the two magnetic phases within each vortex core that we image directly. In a final step, a radiofrequency $\pi/2$ spinor rotation causes each SQV to evolve toward a pair of HQVs. Our creation technique is also distinct from phase-imprinting methods via optical or microwave transitions[23,37,38] or subjecting condensates to artificial gauge fields[39]. We numerically model the experimental conditions of vortex preparation and show how the ferromagnetic interactions influence and complicate the decay process as compared with polar interactions.

Results and discussion

Creation of singular vortices. The BEC wavefunction $\Psi(\mathbf{r}, t)$ is expressed in terms of the atomic spinor $\zeta(\mathbf{r}, t)$ and atom density $n(\mathbf{r}, t)$ in a basis quantized along the z-axis as

$$\Psi(\mathbf{r}, t) = \sqrt{n(\mathbf{r}, t)}\zeta(\mathbf{r}, t) = \sqrt{n(\mathbf{r}, t)}\begin{pmatrix}\zeta_+(\mathbf{r}, t)\\ \zeta_0(\mathbf{r}, t)\\ \zeta_-(\mathbf{r}, t)\end{pmatrix},\ \zeta^\dagger\zeta = 1 \quad (1)$$

The ground state of the system is determined by the sign of the spin-dependent interaction strength c_2 (“Methods”) and the quadratic Zeeman term q, as the linear Zeeman term p does not participate in a system with fixed longitudinal magnetization. In our experiments we have $q > |c_2|n$, specifying an easy-axis polar ground-state phase for ^{87}Rb[1]. In comparison to experiments involving ^{23}Na[9,26], for which $q < |c_2|n$ and the ground-state phase is easy-plane polar[1], we shall see that this introduces significantly different dynamics when $\hat{\mathbf{d}}$ (“Methods”) is not aligned with the magnetic field.

The experiment begins with an optically trapped ferromagnetic ^{87}Rb condensate of $N \sim 2.0 \times 10^5$ atoms (“Methods”). The atoms are exposed to a magnetic field described, in Cartesian coordinates (x, y, z) with respect to the center of the condensate, by

$$\mathbf{B}(t) = B_z(t)\hat{\mathbf{z}} + (x\hat{\mathbf{x}} + y\hat{\mathbf{y}} - 2z\hat{\mathbf{z}})b_q(t), \quad (2)$$

where B_z is the strength of an applied bias field along the z-axis produced by a Helmholtz coil pair, and b_q is the strength of a 3D quadrupole field produced by a coaxial pair of anti-Helmholtz coils. Two other pairs of coils aligned with the x and y directions null those bias field components. The condensate spin is initially aligned along the z-axis, represented by the ferromagnetic spinor $(1, 0, 0)^T$ in the space-fixed basis we adopt for the remaining discussion. At the conclusion of the experiments, described below, the quadrupole field and the optical trap are extinguished, and the spinor components are separated using a Stern–Gerlach separation technique (“Methods”). The atomic density distributions are then simultaneously imaged along the y- and z-axes in a magnetic field aligned with the z-axis.

We use a phase-imprinting process to introduce the polar SQVs, following the vortex creation technique introduced in ref. [12]. A nonsingular vortex is first created by linearly ramping the magnetic bias field B_z to bring the location at which $\mathbf{B}$ vanishes, at $z = B_z/(2b_q)$, entirely through the condensate along the z-axis (“Methods”). The atomic spins incompletely follow this field reorientation[40,41], permitting us to tailor the bending of the magnetization density by selecting the rate at which the zero of the field passes through the condensate. Instead of creating a nonsingular vortex representing a continuous, smooth spin texture, our specific choice triggers an instability that causes the nonsingular vortex to decay into two singular SO(3) vortices in the ferromagnetic phase[12], each described in this basis by $(e^{i\varphi}, 0, 0)^T$ where φ is the azimuthal angle around the vortex line.

In scalar superfluids, a singular defect implies that the superfluid density at the singularity vanishes, but in spinor BECs it is energetically favorable to accommodate the singularity by filling the vortex core with atoms in a different magnetic phase when the spin-dependent interaction is weaker than the spin-independent one[6,8,42]. The vortex-core regions in our experiment thus contain atoms in the nonrotating polar phase, described on this basis by $(0, 1, 0)^T$, as shown in Fig. 1. These exhibit a coherent, stable topological interface between the two distinct magnetic phases[35,36,43], where the magnetic phase changes continuously within the vortex core. Analogous topological interfaces are universal across many areas of physics, ranging from superfluid liquid ^{3}He[44,45] to early-universe cosmology and superstring theory[46,47], as well as to exotic superconductivity[48].

We use a magnetic phase exchange technique to rapidly exchange the polar and ferromagnetic phases. For the texture described above this amounts to swapping the $m = +1$ and $m = 0$ spinor components with a sequence of three resonant microwave π-pulses through an intermediate state (“Methods”), as summarized in Fig. 1a. Afterward, the topological interface between magnetic phases in the vortex core is reversed: along each singularity, the atoms attain the pure ferromagnetic phase $(1, 0, 0)^T$, while the surrounding circulating bulk superfluid is in

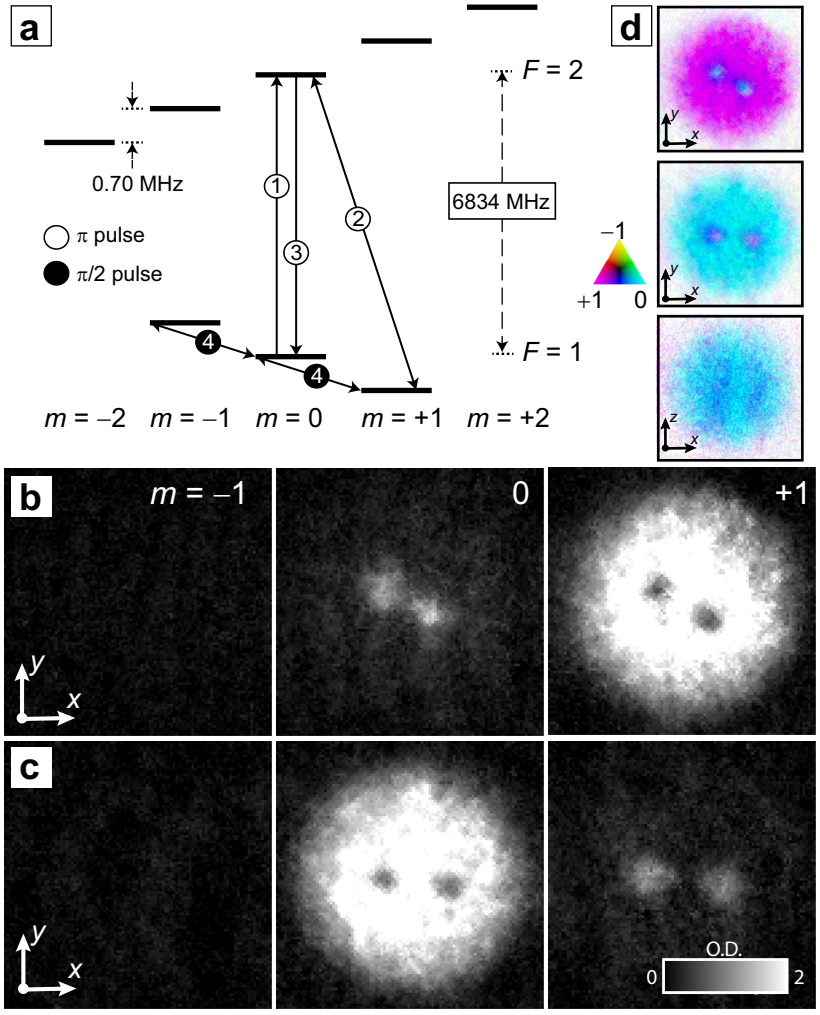

Fig. 1 Creation and detection of the polar singly-quantized vortices (SQVs). a A sequence of microwave π-pulses (open circles 1–3) swaps the $m = +1$ and $m = 0$ spinor components via the $F = 2$, $m = 0$ state, taking the initial pair of SO(3) vortices (**b**) into a pair of polar SQVs with filled ferromagnetic cores (**c**). An optional radiofrequency $\pi/2$-pulse (filled circle 4) rotates the spinor. The respective pulse lengths are (10, 82, 10, 15) μs. **b**, **c** Images of the spinor-component column densities, integrated along the imaging (z) axis before (**b**) and after (**c**) the phase exchange sequence, in units of optical depth (O.D., grayscale bar). **d** False color spinor composition, with a top image of the ferromagnetic SQVs (upper) and top and side images of the polar SQVs (middle and bottom, respectively). Magenta and cyan correspond to pure $m = +1$ and $m = 0$ spinor components, respectively. The field of view in all panel images is 219 μm × 219 μm.

the polar phase $(0, e^{i\varphi}, 0)^T$. These features are clearly seen in Fig. 1b–d. Creation of this vortex state using magnetic phase exchange is one of the principal results of the present study.

Vortex cores and dynamics. We model the two polar SQVs and their ferromagnetic cores numerically in 3D (Fig. 2a–f). Each vortex in the figure represents a polar SQV with a filled core. Analytically, the spinor representing both the vortex and its ferromagnetic core can be constructed as[36]

$$\zeta = \frac{e^{i\varphi}}{2}\begin{pmatrix} \sqrt{2}e^{-i\varphi}\left(D_-\sin^2\frac{\beta}{2} - D_+\cos^2\frac{\beta}{2}\right) \\ -\left(D_- + D_+\right)\sin\beta \\ \sqrt{2}e^{i\varphi}\left(D_-\cos^2\frac{\beta}{2} - D_+\sin^2\frac{\beta}{2}\right) \end{pmatrix}, \quad (3)$$

where $D_\pm = (1 \pm |\langle\hat{\mathbf{F}}\rangle|)^{1/2}$ parameterizes the interpolation between the polar and ferromagnetic phases as $|\langle\hat{\mathbf{F}}\rangle|$ varies from 0 in the bulk to 1 on the vortex line. Here φ again denotes the azimuthal angle around the vortex line, whereas β is the polar angle that determines the order-parameter orientation, varying from $\beta = \pi/2$ away from the vortex line to $\beta = 0$ on the line singularity itself. The initial state is modeled numerically and shown in Fig. 2a, b.

Although the spontaneous breaking of the defect core symmetry in the polar phase and the emergence of HQVs depend nontrivially on the relative interaction strength c_2/c_0[6], this dependence can easily be obscured by the density gradients in a harmonically trapped BEC. Of additional significance is the effect of the applied magnetic field, which can restore the vortex-core isotropy at sufficiently high p and suppress the decay into HQVs at sufficiently high q[49,50]. We find empirically that an applied bias magnetic field of 1 G is sufficient to inhibit evolution of the experimental SQV state depicted in Fig. 1c toward HQVs.

To induce condensate dynamics, we apply a $\pi/2$-pulse within the $F = 1$ manifold to rotate both the nematic director (in the polar phase) and the condensate spin (in the ferromagnetic phase) into the xy plane. The spinor rotation can be understood by describing a single SQV as a vortex line in the $m = 0$ component with core filled by atoms in the $m = +1$ component.

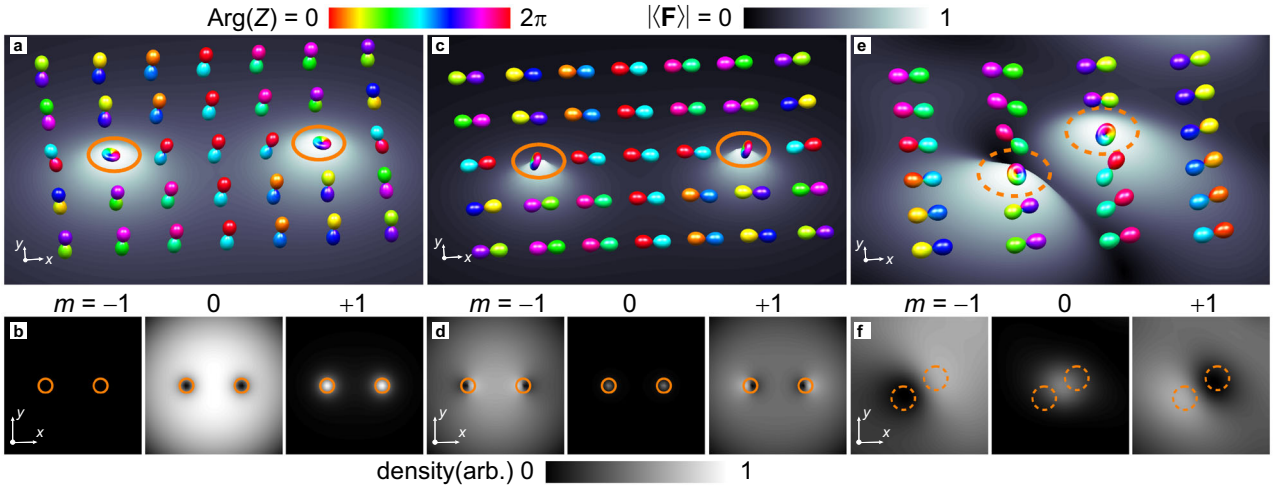

Fig. 2 Theoretical illustrations of the vortex-core structure and order parameter. a Two polar singly-quantized vortices (SQVs) corresponding to Fig. 1c. The background indicates condensate spin magnitude, showing the ferromagnetic cores. The symmetry of the order parameter is represented as the surface of $|Z(\theta,\phi)|^2$, where $Z(\theta,\phi)=\sum_{m=-1}^{+1} Y_{1,m}(\theta,\phi)\zeta_m$ expands the spinor in terms of the spherical harmonics $Y_{1,m}(\theta,\phi)$, parameterized by local spherical coordinates (θ,ϕ). The color map shows Arg(Z) and the upper grayscale bar indicates the spin magnitude. **b** The corresponding spinor components, with density as indicated by the lower grayscale bar. **c**, **d** Same as (**a**, **b**), but after application of a $\pi/2$ spinor rotation. **e**, **f** Expanded view of a single SQV after time evolution, corresponding to the experimental situation in Fig. 4a. The SQV has split into a pair of half-quantum vortices (HQVs). Orange solid (dashed) circles indicate the positions of the SQVs (HQVs).

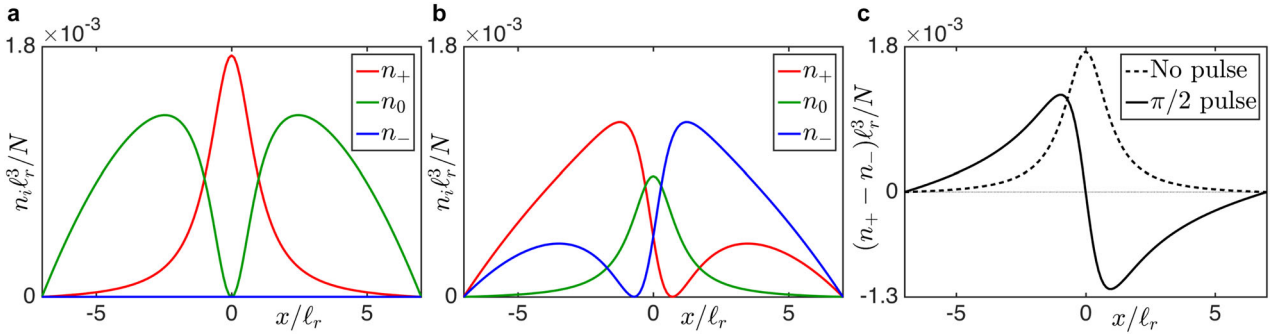

Fig. 3 Analytically constructed cross-sections of spinor component and longitudinal magnetization densities of a singly-quantized vortex (SQV). **a** The spinor components for the initial SQV in the easy-axis polar phase, with red, green, and blue lines corresponding to $m=+1$, 0, and -1, respectively. **b** The spinor components for the SQV after a $\pi/2$ spin rotation to the easy-plane polar phase. Offset phase singularities appear near the center of the plot, where the $m=\pm1$ components (red and blue lines) vanish but the $m=0$ component (green line) does not. **c** Density difference n_+-n_-, to which the longitudinal magnetization density is proportional, before and after the $\pi/2$-pulse. The strongly magnetized regions coincide with the phase singularities in (**b**). Lengths given in units of the transverse trap length $\ell_r=\sqrt{\hbar/(M_a\omega_r)}$ for atomic mass M_a, and N is the number of atoms.

Under a $\pi/2$ spinor rotation about the y axis, the spinor transforms as

$$\begin{pmatrix}\sqrt{1-g(\rho)}\\ e^{i\varphi}\sqrt{g(\rho)}\\ 0\end{pmatrix}\rightarrow\frac{1}{2}\begin{pmatrix}-e^{i\varphi}\sqrt{2g(\rho)}+\sqrt{1-g(\rho)}\\ \sqrt{2-2(\rho)}\\ e^{i\varphi}\sqrt{2g(\rho)}+\sqrt{1-g(\rho)}\end{pmatrix}\qquad(4)$$

where $g(\rho)=\rho^2/(\rho^2+r_0^2)$ approximates the vortex-core profile with size parameterized by r_0. The transformation defined by Eq. (4) is illustrated in Figs. 2c, d and 3a–c. After the rotation, a density maximum in the $m=0$ component appears at the location of the vortex core, bracketed by symmetrically displaced density minima in the $m=\pm1$ spinor components. These spatially offset phase singularities result from the sum of ferromagnetic and polar terms of the initial spinor that transform differently within the vortex core[12]. Note that the spinor wavefunction still contains single SQVs—the presence of the offset phase singularities alone does not imply splitting. In the experiment, we observe these principal features for each of the two created SQVs immediately after the $\pi/2$-pulse (Fig. 4a).

As the system evolves, the spatial separation between the phase singularities associated with both SQVs increases, and each phase singularity grows in size as it fills with fluid in the $m=+1$ (or, for the other of the pair, $m=-1$) spinor component (Fig. 4a–f). These effects can be seen in the emergence of sharply defined proximate bright and dark regions in the total longitudinal magnetization density $M(\mathbf{r})\approx n_{+1}-n_{-1}$, shown in the rightmost column of Fig. 4, as well as directly from the locations of the density minima within the $m=\pm1$ spinor components. The density of the $m=0$ spinor component also becomes more diffuse as the core region of each SQV grows. We stress that the observed vortices exist in a three-dimensional condensate, as confirmed by the examples shown in Fig. 5a–d.

We numerically simulate the dynamics using the coupled Gross–Pitaevskii equations (see "Methods"), also employing an algorithm to restore the conservation of longitudinal magnetization[25] in the presence of a small phenomenological dissipation.

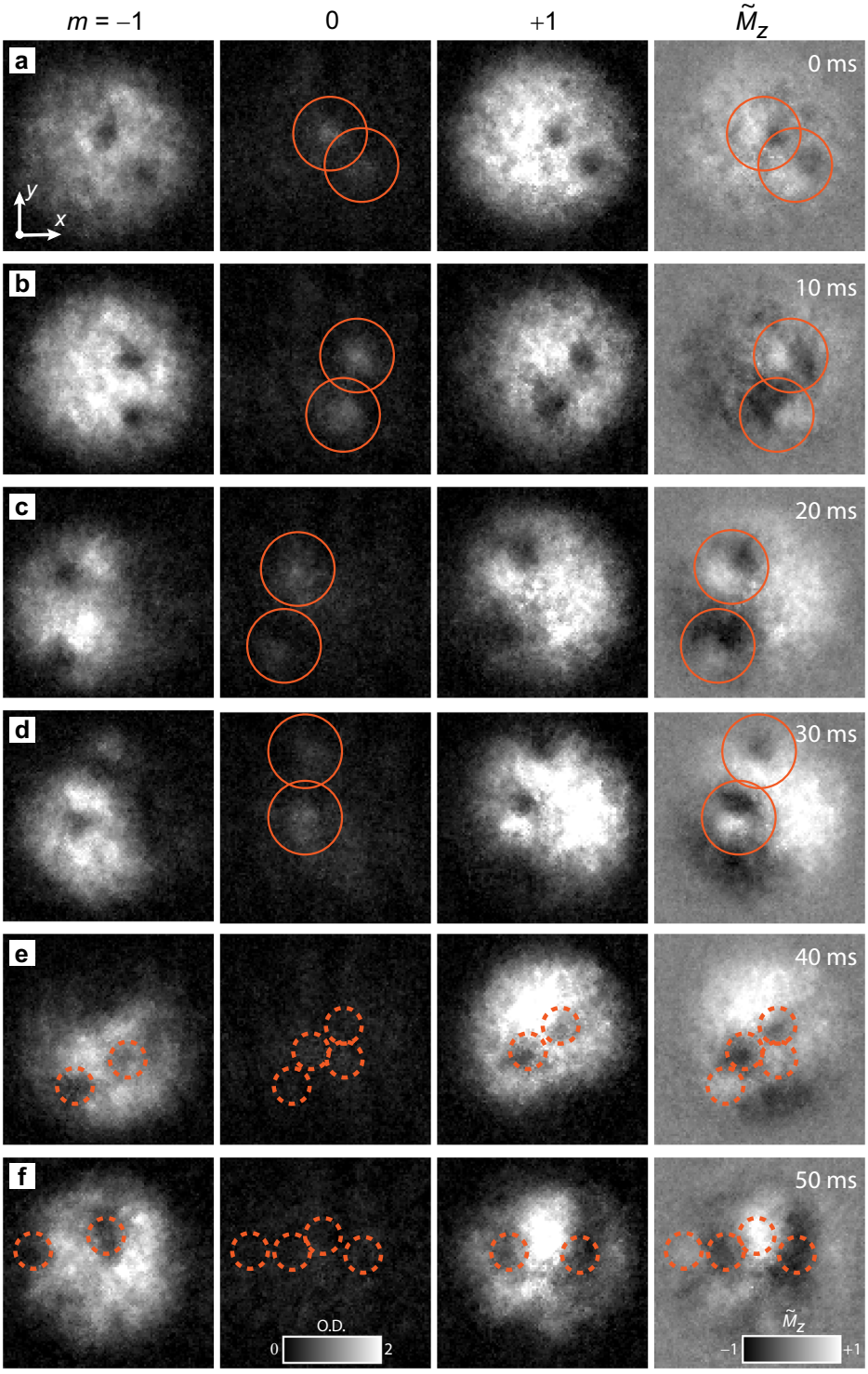

Fig. 4 Time evolution of the singly-quantized vortices after a radiofrequency $\pi/2$-pulse. a–f Images of the spinor-component column densities $\tilde{n}_m$ for $m = -1$, $m = 0$, and $m = -1$, and the longitudinal magnetization column density $\tilde{M}_z = (\tilde{n}_{+1} - \tilde{n}_{-1})$. Panel images in each of (**a**–**f**) are from an individual realization of the experiment with an evolution time of (0, 10, 20, 30, 40, 50) ms after the pulse, respectively. Solid orange circles in (**a**–**d**) indicate identifiable maxima in the $m = 0$ spinor component and are overlaid upon the magnetization image. Dashed orange circles in (**e**, **f**) are estimated locations of offset phase singularities identified from circumscribed density minima in the $m = \pm 1$ spinor components and are similarly overlaid on the $m = 0$ and magnetization images. All densities are integrated along the imaging (z) axis and expressed in units of optical depth (O.D., grayscale bars). The field of view of each image is 219 μm × 219 μm.

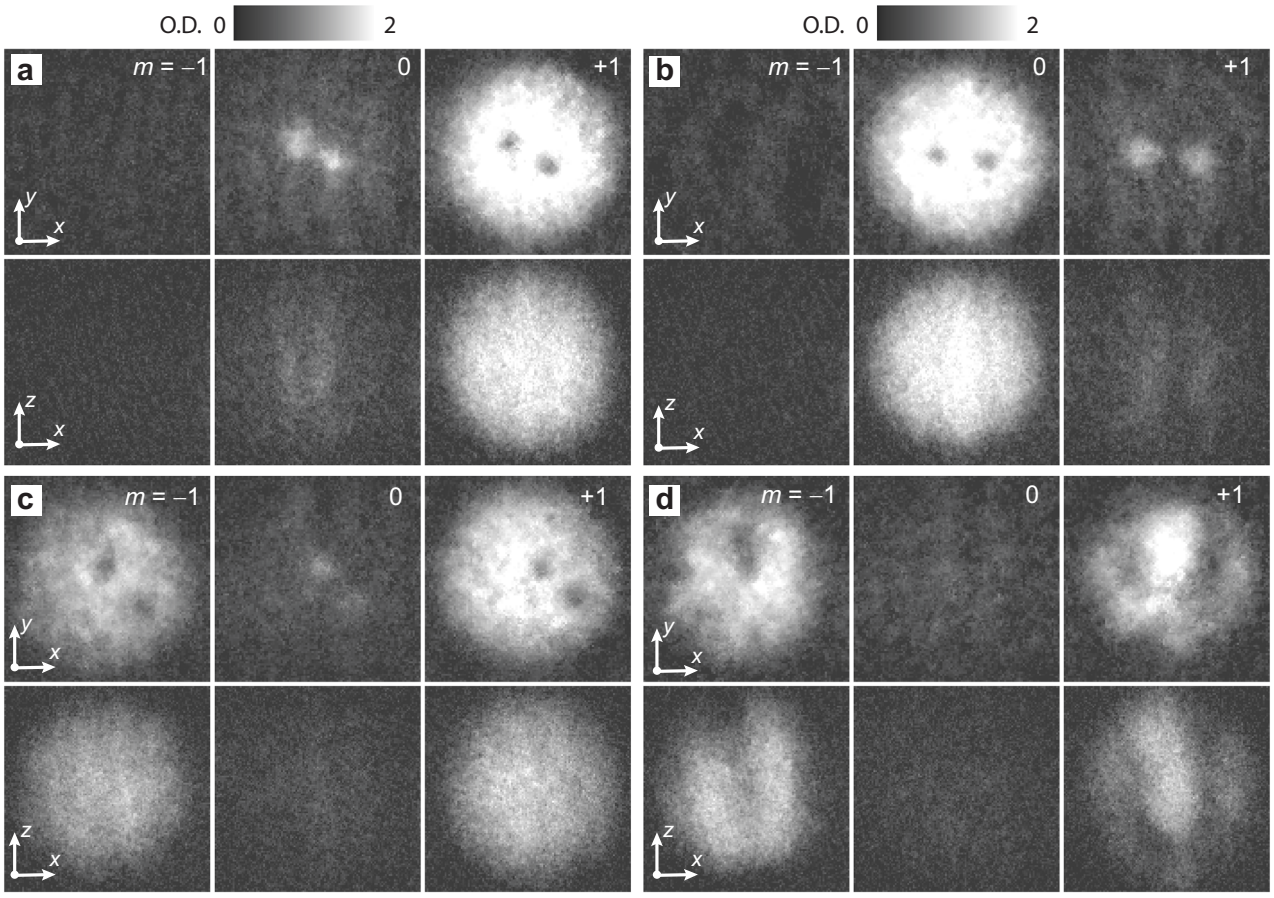

Fig. 5 Three-dimensional nature of several representative condensates with vortices. a The initial SO(3) vortices, after the splitting of the nonsingular texture, with images of the spinor-component column densities taken simultaneously along the *z*- and *y*-axes as indicated by the coordinate arrows. **b** As (**a**) for a pair of polar, singly-quantized vortices (SQVs) after the rapid exchange of the magnetic phases. **c** As (**a**) for two SQVs after rotating the directors into the *xy* plane by the radiofrequency $\pi/2$-pulse. **d** As (**a**) for a likely half-quantum vortex candidate after 50 ms of time evolution following the pulse. Each set of panel images within (**a**–**d**) is from a separate realization of the experiment and shows the spinor-component column densities, integrated along the corresponding imaging axis, with intensity expressed in units of optical depth (O.D., grayscale bar). The field of view of each panel image is 219 μm × 219 μm.

The resulting evolved state is shown in Fig. 2e, where the pair of phase singularities associated with each SQV has formed a split pair of HQVs. In the simulation, the fully separated ferromagnetic cores and the symmetry representation of the wavefunction shown in Fig. 2e, f permit straightforward identification of the HQVs. Once separated, the characteristic size of the filled regions is theoretically established by the spin healing length[6,8], which is much larger than the density healing length.

Experimental interpretation. Connecting the experimentally obtained spinor-component densities to the corresponding vortex states in the simulation requires some care, especially with respect to the presence of the $m = 0$ spinor component. For the given magnetic field direction and the idealized case of pure energy relaxation in a condensate with polar interactions in the easy-plane polar regime, an empty-core SQV is known to relax into a pair of HQVs[8] (Fig. 6a, b). These are readily identified in the simulation by the order-parameter symmetry, also showing continuous deformation to the ferromagnetic vortex core. The vector $\hat{\mathbf{d}}$ remains oriented in the *xy* plane everywhere, yielding a completely depopulated $m = 0$ spinor component and equal bulk densities in the $m = \pm 1$ components. The vortices appear as offset phase singularities in the populated components[5]. In this case, the HQVs can conversely be inferred directly from the component images where the $m = 0$ spinor-component vanishes, as this corresponds directly to the *z*-component of $\hat{\mathbf{d}}$.

For ferromagnetic interactions in the easy-axis polar regime, however, the presence of the phase singularities in regions where the $m = 0$ component is nonzero can indicate either the existence of nonzero transverse spin within the unsplit SQV core (Fig. 6c, d), or the rotation of $\hat{\mathbf{d}}$ out of the *xy* plane in a fully split pair of HQVs (Fig. 6e, f). Dissipation (included phenomenologically in the simulations; see "Methods") causes the condensate to evolve toward the ferromagnetic phase; on the other hand, the Zeeman energy favors rotating $\hat{\mathbf{d}}$ out of the *xy* plane. Both effects may lead to a nonzero density remaining in the $m = 0$ component. Only the disappearance of the $m = 0$ spinor component in the experimental images, implying fully longitudinal spin domains with a director that remains in the *xy* plane, conclusively announces the presence of two HQV. This is approximately the situation in Fig. 4e, f.

There are thus several effects that conspire to complicate the experimental interpretation of our results. First, the offset phase singularities of the two initial singular vortices might closely approach one another, making their disambiguation problematic. Second, the presence of a small and consistent but uncontrolled magnetic field gradient globally shifts the $m = \pm 1$ spinor components with respect to one another, creating less sharply defined

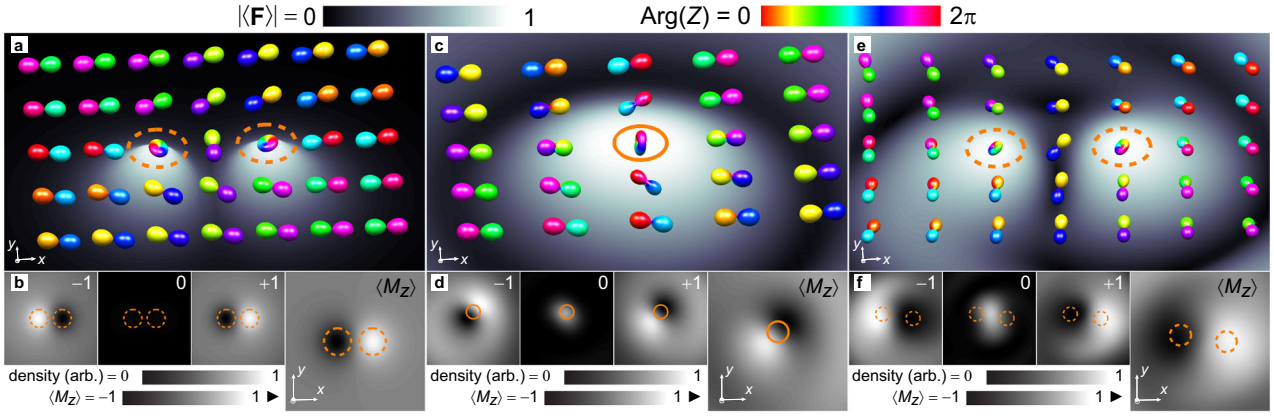

Fig. 6 Numerical simulation of singly-quantized vortex (SQV) core deformation and half-quantum vortex (HQV) formation. a Spin magnitude (background surface, upper grayscale bar) and order-parameter symmetry after pure energy relaxation in a ^{23}Na condensate $c_0/c_2 \simeq 28$) with $q = -0.1\ \hbar\omega_r$, resulting in HQVs. The symmetry of the order parameter is represented as the surface of $|Z(\theta,\phi)|^2$, where $Z(\theta,\phi) = \sum_{m=-1}^{+1} Y_{1,m}(\theta,\phi)\zeta_m$ expands the spinor in terms of the spherical harmonics $Y_{1,m}(\theta,\phi)$, parameterized by local spherical coordinates (θ,ϕ). The color map shows Arg(Z). **b** Corresponding spinor-component densities (labeled by m, middle grayscale bar) and longitudinal magnetization density profile ($\langle M_z\rangle$, lowest grayscale bar). **c**, **d** As (**a**, **b**) for a ^{87}Rb condensate ($c_0/c_2 \simeq -216$) with $q = 0.01\ \hbar\omega_r$ and $\eta = 0.02$. The spinor components exhibit density profiles similar to HQVs even though the vortex has not split. **e**, **f** As (**c**, **d**), but with complete splitting for $q = 0.55\ \hbar\omega_r$, corresponding to the experiment, and $\eta = 0.008$.

regions of opposite longitudinal magnetization density on a size scale comparable to that of the condensate. This effect is pronounced in, e.g., Fig. 4c, d, where the $m = +1$ ($m = -1$) spinor component is shifted to the right (left). Nevertheless, the approximate vortex locations can often be determined by identifying either the density maxima in the $m = 0$ spinor component, as shown in Fig. 4a–d, or the density minima associated with the offset phase singularities in the $m = \pm 1$ spinor components, as suggested by the dashed circles in Fig. 4e, f. The singularities are still difficult to discern if they are near the edge of the condensate, if they are tilted with respect to the imaging axis, or if they exhibit longitudinal (Kelvin wave) excitations[51]. One of the expected singularities in Fig. 4e is less cleanly identified as a result of one or more of these 3D effects.

Concluding remarks. We have implemented a controllable technique of rapid magnetic phase exchange to facilitate the controlled creation of a pair of singular SQVs with nonrotating ferromagnetic cores in the polar magnetic phase of a spin-1 superfluid with ferromagnetic interatomic interactions. Our experimental and theoretical analysis of the decay process in three dimensions suggests the emergence of HQVs. Similar techniques may be used to generate pairs of filled-core vortices in the magnetic phases of spin-2 condensates, where vortex collisions are predicted to possess a non-Abelian character[13,14,16,19] and for which the topological interfaces may lead to exotic phenomena such as vortices with triangular cores[14].

Methods

Experimental details. The condensate begins in an optical trap with frequencies $(\omega_r, \omega_z) = 2\pi(130, 170)\ \mathrm{s}^{-1}$. The axial Thomas–Fermi radius of the condensate is thus 5 μm and the corresponding radial extent is 7 μm. The condensate is exposed to a magnetic field described by Eq. (2), with $B_z(0) = 0.03$ G and $b_q(0) = 4.3(4)$ G/cm, and is initially prepared in the ferromagnetic phase described by the spinor $(1, 0, 0)^{\mathrm{T}}$. To create a nonsingular vortex we ramp B_z to ~ -0.1 G at -5 G/s. Immediately afterward we ramp the field to its minimum value -0.38 G in 10 ms, eliminate the magnetic quadrupole contribution $b_q \to 0$, and adiabatically reorient the field to ~1 G along the $+z$-axis. Over the subsequent 100 ms, the tight bending of the magnetization density causes the nonsingular vortex to decay into two singular SO(3) vortices in the ferromagnetic phase[12].

Swapping the $m = 0$ and $m = +1$ spinor components achieves the exchange of the magnetic phases in this basis (Fig. 1). Our protocol first places the $F = 1$, $m = 0$ spinor component into the $F = 2$, $m = 0$ state using a 10 μs microwave π-pulse at 6834.683197 MHz. The second microwave π-pulse, 82 μs at 6835.391898 MHz, fully exchanges the populations in the $F = 2$, $m = 0$ state and the $F = 1$, $m = 1$ state. The final microwave π-pulse is identical to the first, bringing the population in the $F = 2$, $m = 0$ state to the $F = 1$, $m = 0$ state. The optional radiofrequency $\pi/2$-pulse is 15 μs long at 0.708774 MHz. These frequencies are based on an independent measurement of the magnetic field, which in this case is 1.009 G.

At the conclusion of the experiment, the atoms are released from the trap. A 4.2 ms exposure to a magnetic field gradient of ≈70 G cm^{-1} at the beginning of the subsequent 23 ms expansion separates the spinor components horizontally, after which they are imaged simultaneously along the y- and z-axes.

Numerical model. The Gross–Pitaevskii Hamiltonian density of the spin-1 BEC reads as[1,2]

$$\mathcal{H} = h_0 + \frac{c_0}{2}n^2 + \frac{c_2}{2}n^2|\langle\hat{\mathbf{F}}\rangle|^2 - pn(\hat{\mathbf{e}}_z\cdot\hat{\mathbf{F}}) + qn(\hat{\mathbf{e}}_z\cdot\hat{\mathbf{F}})^2, \quad (5)$$

where we take $h_0 = \frac{\hbar^2}{2M_a}|\nabla\Psi|^2 + V(\mathbf{r})n$ to include the harmonic trapping potential $V(\mathbf{r}) = (M_a\omega_r^2/2)(x^2 + y^2 + 2z^2)$. Here $\hbar$ is the reduced Planck constant, M_a the atomic mass, and ω_r the radial trap frequency. The atomic density is $n = \Psi^\dagger\Psi$, where the spinor wavefunction Ψ is defined in Eq. (1). The condensate spin is the expectation value $\langle\hat{\mathbf{F}}\rangle = \sum_{\alpha\beta}\zeta_\alpha^\dagger\hat{\mathbf{F}}_{\alpha\beta}\zeta_\beta$, where $\hat{\mathbf{F}}$ is a vector of dimensionless spin-1 Pauli matrices. The constants c_0 and c_2 parameterize the spin-independent and spin-dependent interaction strengths, respectively, and $p \propto |\mathbf{B}|$ and $q \propto |\mathbf{B}|^2$ give the linear and quadratic Zeeman energy shifts due to an applied magnetic field $\mathbf{B}$. We employ experimental parameters in the coupled Gross–Pitaevskii equations derived from Eq. (5) to simulate the condensate dynamics. Dissipation is included phenomenologically by setting time to include a small imaginary component $t \to (1 - i\eta)t$, where $\eta \sim 10^{-2}$.

The only spin-flip processes allowed by angular-momentum conservation in s-wave scattering are $2|m = 0\rangle \rightleftharpoons |m = +1\rangle + |m = -1\rangle$. On time scales where s-wave scattering is dominant, this implies that the longitudinal magnetization

$$\langle M_z\rangle = \frac{1}{N}\int d^3r\ n(\mathbf{r})F_z(\mathbf{r}), \quad (6)$$

where F_z is the z-component of the condensate spin, is approximately conserved. Making the Gross–Pitaevskii equations dissipative breaks this conservation law. In our simulations, we therefore combine a split-step method[52] with an algorithm that explicitly conserves the longitudinal magnetization[25].

Magnetic phases. The two distinct ground-state phases in a spin-1 Bose–Einstein condensate at zero field are determined by the sign of the spin-dependent atomic interaction parameter c_2 in Eq. (1). For $c_2 < 0$ (e.g., for ^{87}Rb) the system energy is minimized for $|\langle\hat{\mathbf{F}}\rangle| = 1$, resulting in a ferromagnetic order-parameter space characterized by the group of 3D rotations, SO(3)[53,54]. Contrariwise, for $c_2 > 0$ (e.g., for ^{23}Na) the system energy is minimized for $|\langle\hat{\mathbf{F}}\rangle| = 0$, resulting in a uniaxial nematic (polar) order-parameter space characterized by $[S^2 \times \mathrm{U}(1)]/\mathbb{Z}_2$ with local U(1) phase τ and nematic axis $\hat{\mathbf{d}}$[5,55,56], defined implicitly by

$$\zeta_P = \frac{e^{i\tau}}{\sqrt{2}}\begin{pmatrix} -d_x + id_y \\ \sqrt{2}d_z \\ d_x + id_y \end{pmatrix}. \quad (7)$$

The two-element factor group $\mathbb{Z}_2$ appears due to the symmetry $\hat{\mathbf{d}}e^{i\tau} = -\hat{\mathbf{d}}e^{i(\tau+\pi)}$. It is this symmetry that permits vortices in the polar phase to carry half-integer circulation when τ runs between 0 and π around the vortex singularity and $\hat{\mathbf{d}}$ concurrently rotates by π.

At stronger fields with fixed longitudinal magnetization, the quadratic Zeeman term q becomes important for determining the ground state[57–60], and within the polar phase itself there arise two relevant phases: the easy-axis polar, where $\hat{\mathbf{d}}$ is aligned with an applied magnetic field, and the easy-plane polar, where $\hat{\mathbf{d}}$ is perpendicular to the applied magnetic field. In our experiment $q > |c_2|n$, specifying an easy-axis polar ground-state phase.

The order-parameter symmetry in Figs. 2 and 6 is given as the surface of $|Z(\theta,\phi)|^2$, where $Z(\theta,\phi) = \sum_{m=-1}^{+1} Y_{1,m}(\theta,\phi)\zeta_m$ expands the spinor in terms of the spherical harmonics $Y_{1,m}(\theta,\phi)$, parameterized by local spherical coordinates (θ,ϕ), with gauge color given by $\mathrm{Arg}(Z)$.

Data availability

All relevant datasets generated during and/or analyzed during the current study are available from the corresponding author upon request. The source data underlying Figs. 1–6 are provided as a Source data file in the Zenodo repository (doi:10.5281/zenodo.4384683) (ref. [61]).

Code availability

The code is available upon reasonable request.

Received: 6 October 2020; Accepted: 12 February 2021;
Published online: 12 March 2021

References

1. Kawaguchi, Y. & Ueda, M. Spinor Bose–Einstein condensates. *Phys. Rep.* **520**, 253–382 (2012).
2. Stamper-Kurn, D. M. & Ueda, M. Spinor Bose gases: symmetries, magnetism, and quantum dynamics. *Rev. Mod. Phys.* **85**, 1191–1244 (2013).
3. Volovik, G. E. *The Universe in a Helium Droplet* (Oxford University Press, 2003).
4. Vollhardt, D. & Wölfle, P. *The Superfluid Phases of Helium 3* (Taylor & Francis Ltd, 1990).
5. Leonhardt, U. & Volovik, G. How to create an Alice string (half-quantum vortex) in a vector Bose–Einstein condensate. *JETP Lett.* **72**, 46–48 (2000).
6. Ruostekoski, J. & Anglin, J. R. Monopole core instability and Alice rings in spinor Bose–Einstein condensates. *Phys. Rev. Lett.* **91**, 190402 (2003).
7. Ji, A.-C., Liu, W. M., Song, J. L. & Zhou, F. Dynamical creation of fractionalized vortices and vortex lattices. *Phys. Rev. Lett.* **101**, 010402 (2008).
8. Lovegrove, J., Borgh, M. O. & Ruostekoski, J. Energetically stable singular vortex cores in an atomic spin-1 Bose–Einstein condensate. *Phys. Rev. A* **86**, 013613 (2012).
9. Seo, S. W., Kang, S., Kwon, W. J. & Shin, Y.-i Half-quantum vortices in an antiferromagnetic spinor Bose–Einstein condensate. *Phys. Rev. Lett.* **115**, 015301 (2015).
10. Autti, S. et al. Observation of half-quantum vortices in topological superfluid ^{3}He. *Phys. Rev. Lett.* **117**, 255301 (2016).
11. Kang, S., Seo, S. W., Takeuchi, H. & Shin, Y. Observation of wall-vortex composite defects in a spinor Bose–Einstein condensate. *Phys. Rev. Lett.* **122**, 095301 (2019).
12. Weiss, L. S. et al. Controlled creation of a singular spinor vortex by circumventing the Dirac belt trick. *Nat. Commun.* **10**, 4772 (2019).
13. Kobayashi, M., Kawaguchi, Y., Nitta, M. & Ueda, M. Collision dynamics and rung formation of non-Abelian vortices. *Phys. Rev. Lett.* **103**, 115301 (2009).
14. Borgh, M. O. & Ruostekoski, J. Core structure and non-Abelian reconnection of defects in a biaxial nematic spin-2 Bose–Einstein condensate. *Phys. Rev. Lett.* **117**, 275302 (2016).
15. Mawson, T., Ruben, G. & Simula, T. Route to non-Abelian quantum turbulence in spinor Bose–Einstein condensates. *Phys. Rev. A* **91**, 063630 (2015).
16. Semenoff, G. W. & Zhou, F. Discrete symmetries and 1/3–quantum vortices in condensates of $F = 2$ cold atoms. *Phys. Rev. Lett.* **98**, 100401 (2007).
17. Barnett, R., Turner, A. & Demler, E. Classifying vortices in $S = 3$ Bose–Einstein condensates. *Phys. Rev. A* **76**, 013605 (2007).
18. Borgh, M. O., Lovegrove, J. & Ruostekoski, J. Internal structure and stability of vortices in a dipolar spinor Bose–Einstein condensate. *Phys. Rev. A* **95**, 053601 (2017).
19. Mawson, T., Petersen, T. C., Slingerland, J. K. & Simula, T. P. Braiding and fusion of non-abelian vortex anyons. *Phys. Rev. Lett.* **123**, 140404 (2019).
20. Mizushima, T., Machida, K. & Kita, T. Mermin–Ho vortex in ferromagnetic spinor Bose–Einstein condensates. *Phys. Rev. Lett.* **89**, 030401 (2002).
21. Martikainen, J.-P., Collin, A. & Suominen, K.-A. Coreless vortex ground state of the rotating spinor condensate. *Phys. Rev. A* **66**, 053604 (2002).
22. Leanhardt, A. E., Shin, Y., Kielpinski, D., Pritchard, D. E. & Ketterle, W. Coreless vortex formation in a spinor Bose–Einstein condensate. *Phys. Rev. Lett.* **90**, 140403 (2003).
23. Leslie, L. S., Hansen, A., Wright, K. C., Deutsch, B. M. & Bigelow, N. P. Creation and detection of skyrmions in a Bose–Einstein condensate. *Phys. Rev. Lett.* **103**, 250401 (2009).
24. Choi, J.-y et al. Imprinting skyrmion spin textures in Bose–Einstein condensates. *New J. Phys.* **14**, 053013 (2012).
25. Lovegrove, J., Borgh, M. O. & Ruostekoski, J. Energetic stability of coreless vortices in spin-1 Bose–Einstein condensates with conserved magnetization. *Phys. Rev. Lett.* **112**, 075301 (2014).
26. Seo, S. W., Kwon, W. J., Kang, S. & Shin, Y. Collisional dynamics of half-quantum vortices in a spinor Bose–Einstein condensate. *Phys. Rev. Lett.* **116**, 185301 (2016).
27. Thuneberg, E. V. Identification of vortices in superfluid ^{3}He-*B*. *Phys. Rev. Lett.* **56**, 359–362 (1986).
28. Salomaa, M. M. & Volovik, G. E. Vortices with spontaneously broken axisymmetry in ^{3}He-*B*. *Phys. Rev. Lett.* **56**, 363–366 (1986).
29. Kondo, Y. et al. Direct observation of the nonaxisymmetric vortex in superfluid ^{3}He-*B*. *Phys. Rev. Lett.* **67**, 81–84 (1991).
30. Rosenbusch, P., Bretin, V. & Dalibard, J. Dynamics of a single vortex line in a Bose–Einstein condensate. *Phys. Rev. Lett.* **89**, 200403 (2002).
31. Neely, T. W., Samson, E. C., Bradley, A. S., Davis, M. J. & Anderson, B. P. Observation of vortex dipoles in an oblate Bose–Einstein condensate. *Phys. Rev. Lett.* **104**, 160401 (2010).
32. Tilley, D. R. & Tilley, J. *Superfluidity and Superconductivity* 3rd edn (IOP Publishing Ltd, 1990).
33. Weiler, C. N. et al. Spontaneous vortices in the formation of Bose–Einstein condensates. *Nature* **455**, 948–951 (2008).
34. Freilich, D. V., Bianchi, D. M., Kaufman, A. M., Langin, T. K. & Hall, D. S. Real-time dynamics of single vortex lines and vortex dipoles in a Bose–Einstein condensate. *Science* **329**, 1182–1185 (2010).
35. Borgh, M. O. & Ruostekoski, J. Topological interface engineering and defect crossing in ultracold atomic gases. *Phys. Rev. Lett.* **109**, 015302 (2012).
36. Lovegrove, J., Borgh, M. O. & Ruostekoski, J. Stability and internal structure of vortices in spin-1 Bose–Einstein condensates with conserved magnetization. *Phys. Rev. A* **93**, 033633 (2016).
37. Matthews, M. R. et al. Vortices in a Bose–Einstein condensate. *Phys. Rev. Lett.* **83**, 2498–2501 (1999).
38. Andersen, M. F. et al. Quantized rotation of atoms from photons with orbital angular momentum. *Phys. Rev. Lett.* **97**, 170406 (2006).
39. Chen, P.-K. et al. Rotating atomic quantum gases with light-induced azimuthal gauge potentials and the observation of the Hess–Fairbank effect. *Phys. Rev. Lett.* **121**, 250401 (2018).
40. Nakahara, M., Isoshima, T., Machida, K., Ogawa, S.-i & Ohmi, T. A simple method to create a vortex in Bose–Einstein condensate of alkali atoms. *Physica B* **284–288**, 17–18 (2000).
41. Pietilä, V. & Möttönen, M. Creation of Dirac monopoles in spinor Bose–Einstein condensates. *Phys. Rev. Lett.* **103**, 030401 (2009).
42. Kobayashi, S., Kawaguchi, Y., Nitta, M. & Ueda, M. Topological classification of vortex-core structures of spin-1 Bose–Einstein condensates. *Phys. Rev. A* **86**, 023612 (2012).
43. Kasamatsu, K., Takeuchi, H., Nitta, M. & Tsubota, M. Analogues of d-branes in Bose-Einstein condensates. *J. High Energy Phys.* **011**, 068 (2010).
44. Finne, A. P. et al. Dynamics of vortices and interfaces in superfluid ^{3}He. *Rep. Prog. Phys.* **69**, 3157–3230 (2006).
45. Bradley, D. I. et al. Relic topological defects from brane annihilation simulated in superfluid ^{3}He. *Nat. Phys.* **4**, 46–49 (2008).
46. Kibble, T. W. B. Topology of cosmic domains and strings. *J. Phys. A Math. Gen.* **9**, 1387–1398 (1976).
47. Sarangi, S. & Tye, S.-H. H. Cosmic string production towards the end of brane inflation. *Phys. Lett. B* **536**, 185–192 (2002).
48. Bert, J. A. et al. Direct imaging of the coexistence of ferromagnetism and superconductivity at the $LaAlO_3/SrTiO_3$ interface. *Nat. Phys.* **7**, 767–771 (2011).
49. Borgh, M. O., Nitta, M. & Ruostekoski, J. Stable core symmetries and confined textures for a vortex line in a spinor Bose–Einstein condensate. *Phys. Rev. Lett.* **116**, 085301 (2016).
50. Underwood, A. P. C., Baillie, D., Blakie, P. B. & Takeuchi, H. Properties of a nematic spin vortex in an antiferromagnetic spin-1 Bose–Einstein condensate. *Phys. Rev. A* **102**, 023326 (2020).
51. Bretin, V., Rosenbusch, P., Chevy, F., Shlyapnikov, G. V. & Dalibard, J. Quadrupole oscillation of a single-vortex Bose–Einstein condensate: Evidence for Kelvin modes. *Phys. Rev. Lett.* **90**, 100403 (2003).

52. Javanainen, J. & Ruostekoski, J. Symbolic calculation in development of algorithms: split-step methods for the Gross–Pitaevskii equation. *J Phys A: Math Gen* **39**, L179–L184 (2006).
53. Ho, T.-L. Spinor Bose condensates in optical traps. *Phys. Rev. Lett.* **81**, 742–745 (1998).
54. Ohmi, T. & Machida, K. Bose–Einstein condensation with internal degrees of freedom in alkali atom gases. *J. Phys. Soc. Jpn.* **67**, 1822–1825 (1998).
55. Zhou, F. Spin correlation and discrete symmetry in spinor Bose–Einstein condensates. *Phys. Rev. Lett.* **87**, 080401 (2001).
56. Zhou, F. Quantum spin nematic states in Bose–Einstein condensates. *Int. J. Mod. Phys. B* **17**, 2643–2698 (2003).
57. Zhang, W., Yi, S. & You, L. Mean field ground state of a spin-1 condensate in a magnetic field. *New J. Phys.* **5**, 77 (2003).
58. Murata, K., Saito, H. & Ueda, M. Broken-axisymmetry phase of a spin-1 ferromagnetic Bose–Einstein condensate. *Phys. Rev. A* **75**, 013607 (2007).
59. Sadler, L. E., Higbie, J. M., Leslie, S. R., Vengalattore, M. & Stamper-Kurn, D. M. Spontaneous symmetry breaking in a quenched ferromagnetic spinor Bose–Einstein condensate. *Nature* **443**, 312–315 (2006).
60. Ruostekoski, J. & Dutton, Z. Dynamical and energetic instabilities in multicomponent Bose–Einstein condensates in optical lattices. *Phys. Rev. A* **76**, 063607 (2007).
61. Xiao, Y. et al. Controlled creation and decay of singly-quantized vortices in a polar magnetic phase. Zenodo digital repository. doi:10.5281/zenodo.4384683 (2020).

Acknowledgements

We gratefully acknowledge experimental assistance from and helpful conversations with T. Ollikainen. D.S.H. acknowledges financial support from the National Science Foundation (Grant No. PHY-1806318.) and J.R. from the UK EPSRC (Grant Nos. EP/P026133/1, EP/S002952/1). The numerical computations were performed using the High Performance Computing Cluster supported by the Research and Specialist Computing Support service at the University of East Anglia.

Author contributions

Y.X., L.S.W., A.A.B., and D.S.H. developed and conducted the experiments and analyzed the data. Numerical simulations were carried out by M.O.B., and the theoretical analysis was developed by M.O.B. and J.R. The manuscript was written by M.O.B., J.R., and D.S.H. All authors discussed the results and commented on the manuscript.

Competing interests

The authors declare no competing interests.

Additional information

Correspondence and requests for materials should be addressed to D.S.H.

Reprints and permission information is available at http://www.nature.com/reprints

Publisher's note Springer Nature remains neutral with regard to jurisdictional claims in published maps and institutional affiliations.